



OPEN Sedimentary provenance supports a mid-paleozoic tectonic connection between the Junggar and Altai terranes in central Asia

Di Li^{1,3}✉, Yigui Han²✉, Guochun Zhao^{2,3}, Mei-Fu Zhou^{3,4}, Dengfa He¹, Shuoqin Hou¹, Yu Zhen¹, Dan Fan¹ & Hao Yang¹

The provenance of Precambrian detritus in the Junggar and Altai terranes provides crucial constraints on the peri-Siberian accretionary tectonic evolution in the middle Paleozoic. The Precambrian detrital zircons have no coeval magmatic equivalents in the Junggar terrane but show U–Pb age spectra and $\epsilon_{\text{Hf}}(t)$ values comparable to those in the Altai terrane. The correlations suggest that the old detrital materials in the Junggar and Altai terranes were most likely derived from the Siberia craton and adjacent Tuva-Mongolian microcontinent. Paleozoic zircons in the Junggar terrane display a $\epsilon_{\text{Hf}}(t)$ pattern from large spread to dominantly positive values at ca. 420–410 Ma. Such an abrupt change points to an accretionary tectonic transition from an advancing to retreating mode during mid-Paleozoic time, synchronous with similar tectonic switch occurring in the Altai terrane. Taking into account the temporal and spatial relations in sedimentation, tectonism and arc magmatism, we propose that the Junggar terrane had once collided onto the peri-Siberian Altai terrane to receive abundant old detritus from the Siberian continent in the Silurian–early Devonian. They were subsequently separated at ca. 420–410 Ma, possibly due to the slab rollback of the subducting Paleo-Asian Ocean (PAO) plate. These results constrain an Early Paleozoic tectono-paleogeographic boundary of the CAO along the North Tianshan–Solonker suture zone, and also imply a long-lived PAO subduction was responsible for the Neoproterozoic to Paleozoic accretionary orogenesis at the margins of southern Siberia, eastern Kazakhstan, and northern Gondwana.

Keywords Source-to-sink relationship, Terrane amalgamation, Accretionary tectonic transition, Early paleozoic, Southern CAO

Paleozoic evolution of the Paleo-Asian Ocean (PAO) involved the development of the Siberian accretionary margin and the addition of a range of blocks from the Gondwana northern margin, which were finally amalgamated in the Permo-Triassic to form the Central Asian Orogenic Belt (CAOB)^{1,2} (Fig. 1a) and thus shaped the main body of Pangea^{3–5}. At this time, numerous peri-Siberian juvenile terranes (e.g., Junggar and Altai), in accompany with the Gondwana-derived blocks (e.g., Tarim), travelled north to progressively collide with the Siberian margin, leading to multiple-stage orogenic events^{6–8}. The paleopositions of these juvenile terranes is poorly constrained due to lack available paleomagnetic data. The Altai terrane was likely located near the peri-Siberian accretionary margin during the Paleozoic^{6,9}, but the Junggar terrane has been placed at the Tarim northern margin¹⁰ or within the PAO realm throughout the Paleozoic¹, even on the Siberian margin in the mid-Paleozoic¹¹. Therefore, understanding its Caledonian-age interaction with the Gondwana-derived block and the Siberian margin is vital for the reconstruction of central Asia.

The Junggar terrane is widely considered as a conjoined terrane mainly consisting of two independent units until the late Paleozoic² (Fig. 1b), whereas some scholars treated it as an integral block in the early Paleozoic¹¹. Recent data indicate that the Paleozoic strata of the Junggar terrane contain abundant Precambrian detrital

¹Key Laboratory of Marine Reservoir Evolution and Hydrocarbon Accumulation Mechanism, The Ministry of Education, School of Energy Resources, China University of Geosciences, Beijing 100083, China. ²State Key Laboratory of Continental Dynamics, Department of Geology, Northwest University, Xi'an 710069, China. ³Department of Earth Sciences, The University of Hong Kong, Hong Kong, China. ⁴State Key Laboratory of Ore Deposit Geochemistry, Institute of Geochemistry, Chinese Academy of Sciences, Guiyang 550081, China. ✉email: lidi@cugb.edu.cn; hanyigui@nwu.edu.cn

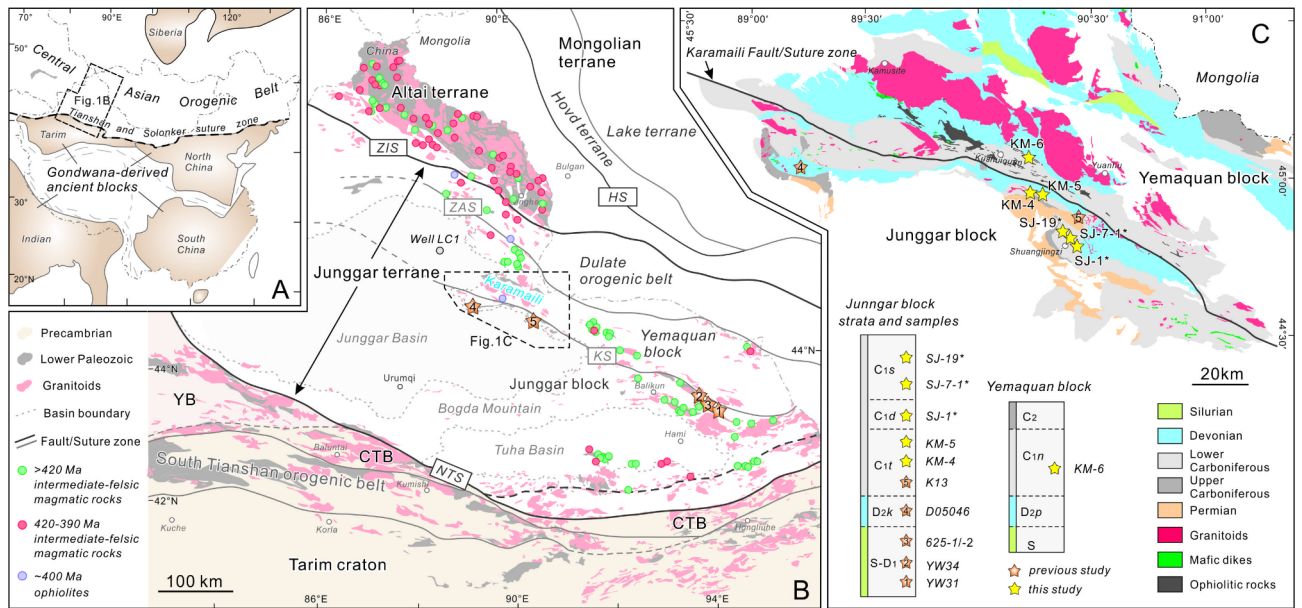


Fig. 1. (a) Overview map showing relationship of the study area with the Central Asian Orogenic Belt (modified after Windley et al.¹, Zhao et al.⁵). (b) Schematic geological map of Junggar-Altai terrane and adjacent regions (modified after Chen and Jahn⁶³, Badarch et al.²¹, Li et al.²³), showing the main tectonic units and the age and distribution of the Early-Late Paleozoic magmatic rocks. (c) Geological map in the Karamaili area with sample locations of the compiled data. HS—Hovd suture zone; ZIS—Irtys suture zone; ZAS—Zhaheba–Aermantai suture zone; KS—Karamaili suture zone; NTS—North Tianshan suture zone; YB—Yili block; CTB—Central Tianshan block. This figure is generated using CorelDRAW X8 created by the CorelDRAW Team under an open license (<http://www.coreldraw.com/cn/product/graphic-design-software/>).

materials like the Altai terrane^{12,13}. However, the provenance of these ancient detrital and associated tectonism remains enigmatic. The combined U–Pb and Lu–Hf analysis of detrital zircons is probably an effective approach to solve the tectonic-sedimentary coupling problem because it has been widely applied to trace sedimentary provenance and determine tectonic transition processes¹⁴.

In this study, we reveal derivation of the Precambrian detrital materials in the Junggar terrane from the Siberia craton and adjacent Tuva-Mongolian microcontinent, as well as middle Paleozoic switching accretionary tectonics of the Junggar terrane, based on new and compiled zircon U–Pb–Hf data. We link the source-to-sink system and the accretionary tectonics with the relations among Junggar terrane, Altai terrane and Siberian continent, disclosing a short-lived connection between the unified Junggar-Altai terrane and the Siberian margin during mid-Paleozoic time. Our results offer new constraints on the paleogeographic reconstruction of the southern CAO, promoting the understanding of the Pangea assembly.

Geological background

The CAO is situated between the Siberia and Baltica cratons to the north and the Tarim and North China cratons to the south (Fig. 1a), and it underwent prolonged subduction-accretion processes during the evolution of the PAO from the Neoproterozoic to the late Paleozoic¹. Tectonically, this belt can be divided into the Mongolia and the Kazakhstan collage systems². The Mongolia collage system is presently south of the Siberia craton and comprises juvenile terranes (e.g., Altai, Hovd and Lake, Fig. 1b) and some Precambrian continental blocks (e.g., Tuva-Mongolian, Zavkhan and Baydrag). Several episodes of magmatic activities from the Archean to the Paleozoic are recorded in the western Mongolia and/or the Siberia craton¹⁵. It is generally suggested that the amalgamation events from the Altai-Mongolian terrane to the south margin of Siberia craton have occurred in the Early–Middle Paleozoic, leading to the formation of the Carysh-Terekta-Ulagan-Sanyan suture zone in the Altai-Sayan region and Ol’Khon suture zone in the Baikal region^{16–18}.

The Junggar terrane is bounded to the south by the North Tianshan suture zone, marking the site of closure of a PAO branch (i.e., North Tianshan Ocean) and collision with the Tarim craton and neighboring Central Tianshan block (CTB) (Fig. 1b). Both the Tarim craton and the CTB preserve a crystalline Precambrian basement and the Neoproterozoic and Paleozoic subduction-related tectono-magmatic records^{19,20}. By the Irtys suture zone to its north, the Junggar terrane is separated from the Altai terrane at the western margin of the Tuva-Mongolian terrane²¹, and this study mainly focused on the eastern Junggar terrane because the western Junggar experienced different evolution in the Paleozoic² (Fig. 1b). The Junggar terrane, as an accretionary orogen related to the evolution of the PAO¹, was formed by the amalgamation of multiple linear tectonic units including the Junggar block, the Yemaquan block, the Dulate orogenic belt and their intervening Karamaili and Zhaheba–Aermantai suture zones. There are abundant Paleozoic ophiolitic rocks along four suture zones (NTS, KS, ZAS and ZIS) in the Junggar-Altai region (Fig. 1b). The ages of the North Tianshan ophiolites have an almost continuous span of

494–325 Ma relative to those in other zones that are concentrated in the two periods of 503–481 Ma and 409–364 Ma²². Numerous and widespread Paleozoic magmatism took place in the Junggar and Altai terranes (Fig. 1b). The intermediate-felsic magmatic rocks commonly have arc affinities, suggesting a long-lived accretionary history that may extend at least to the Late Carboniferous^{2,23}.

Unlike the Tarim craton and its neighbor, the Junggar and Altai terranes were underlain mainly by juvenile crust and lack large Precambrian basement rocks²⁴. These two terranes have comparable Paleozoic tectonostratigraphic sequences, characterized by the deformed/metamorphosed Early Paleozoic strata and unconformably overlying Devonian–Carboniferous strata. The Lower Paleozoic is represented by the Huangcaopo and Kubusu Groups of the Junggar terrane and the Habaha and Kulumudi Groups of the Chinese Altai terrane, consisting mainly of marine volcano-siliciclastic rocks^{13,25}. The dating results suggest that they were probably deposited in the Silurian to early Devonian^{13,26}. Abundant Precambrian detrital materials are involved in these sedimentary rocks^{13,26–28}. Immediately above the unconformity are the Early Devonian rift successions^{23,29}, accompanied by the development of rift magmatic rocks^{30–32}. This unconformity is also recorded in the Tuva–Mongolian terrane and it interrupted the Cambrian–Ordovician carbonate-clastic deposition, forming the Silurian volcanoclastic flyschoid sequences with minor conglomerate layers²¹. Recent study shows that the late Ordovician–Silurian tectonic contraction may take place in the Junggar terrane, which induced ca. 450–420 Ma crustal thickening-related magmatism across the Karamaili suture zone²².

In the mid-Carboniferous, the Karamaili ocean that opened in the early Devonian was the first to close relative to others³³ (Fig. 1b), resulting in the amalgamation of the Junggar and Yemaquan blocks to create the Junggar terrane. The Carboniferous sedimentary rocks recorded local Paleozoic magmatism in the terrane and earlier allochthonous Precambrian detritus. In this paper, we undertook detrital zircon U–Pb–Hf analyses for six Lower Carboniferous sandstone samples collected from the Shuangjingzi and Kushuiquan domains in the Junggar terrane (Figs. 1c and 2).

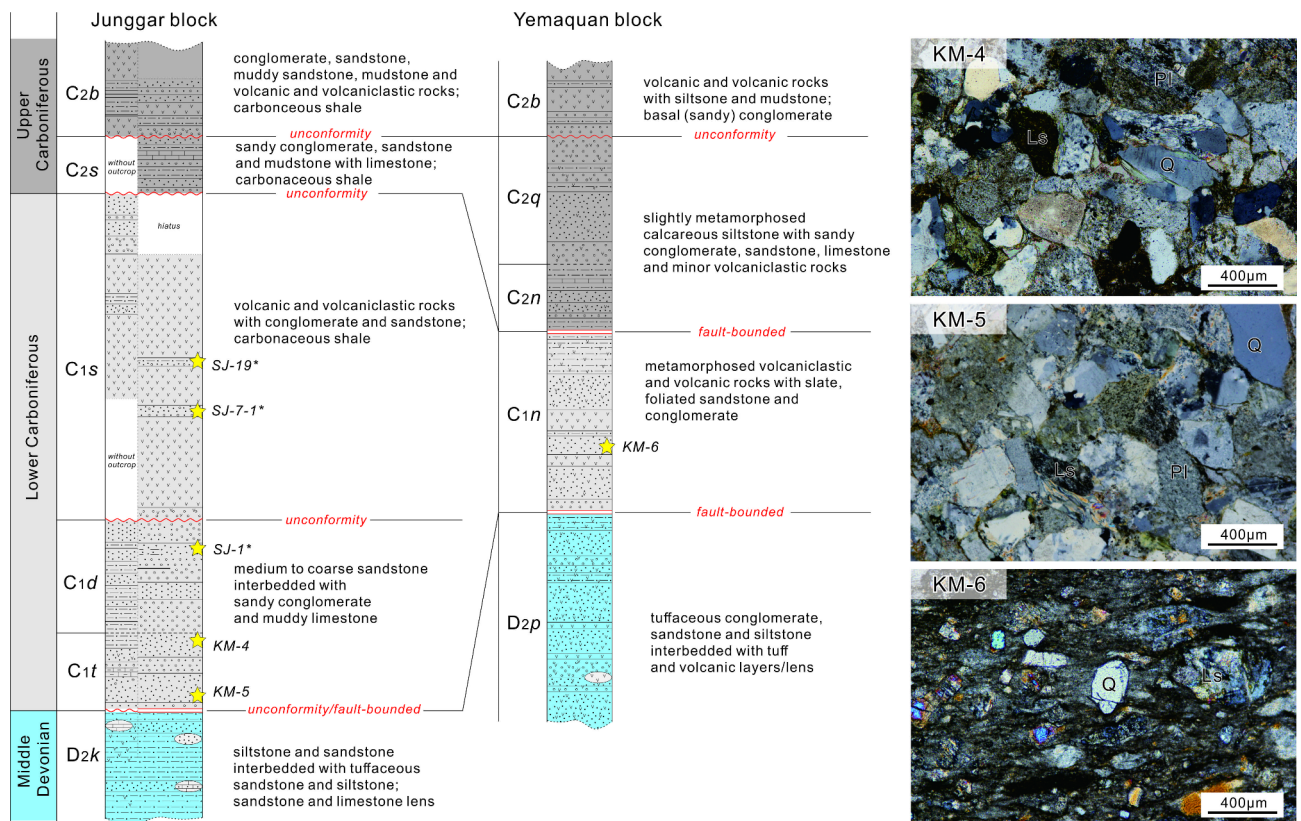


Fig. 2. Comprehensive stratigraphic column for lithology and sampling sites and photomicrographs of the Early Carboniferous sandstones from the northern margin of the Junggar block and the southern margin of the Yemaquan block. D_{2k} = Middle Devonian Karamaili Formation; D_{2p} = Middle Devonian Pingdingshan Formation; C_{1t} = Lower Carboniferous Tamugang Formation; C_{1d} = Lower Carboniferous Dishuiquan Formation; C_{1s} = Lower Carboniferous Songkaersu Formation; C_{1n} and C_{2n} = Lower Carboniferous Nanmingshui Formation (lower and upper part); C_{2s} = Upper Carboniferous Shuangjingzi Formation; C_{2q} = Upper Carboniferous Qingshui Formation; C_{2b} = Upper Carboniferous Batamayineishan Formation; Q = quartz; Pl = plagioclase; Ls = lithic shards. The locations of the samples with (*) are from Li et al.³³.

Results

Detrital zircon U–Pb geochronology and Lu–Hf isotopic compositions

Detrital zircons from the Lower Carboniferous samples are colorless, transparent and prismatic with variable length/width ratios (1.0–3.0). Zircons with Paleozoic ages commonly show more euhedral/subhedral shapes and larger aspect ratios relative to Precambrian zircons. Almost all analyzed zircons have high Th/U ratios (> 0.1 , Fig. 3f) and most of them possess oscillatory zoning under the cathodoluminescence (CL) images (Fig. S1), indicating a magmatic origin. Two Tamugang Formation (C_1t) samples (KM-4 and KM-5) from the northern margin of the Junggar block yield 139 concordant detrital zircon U–Pb ages ranging from 348 ± 3 Ma to 3539 ± 30 Ma (Fig. 3a, b; Table S1). Their spectrum exhibits a major Paleozoic age population at ~ 350 – 520 Ma and some Precambrian age clusters around 740–910 Ma, 1150–1490 Ma, 2.3 Ga, 2.9 Ga and 3.5 Ga, almost identical to the Lower Carboniferous and Middle Devonian samples (Fig. 3c, d and S2). One Namingshui Formation (C_{1n}) sample (KM-6) from the southern margin of the Yemaquan block give consistent prominent Paleozoic age population, and a few Precambrian ages at ~ 760 Ma and ~ 2.6 Ga (Fig. 3e; Table S1). A total of 1004 (new and compiled) detrital zircon U–Pb dating results of the Middle Devonian–Lower Carboniferous strata from the two block margins (i.e., across the Karamaili suture zone) are dominated by Paleozoic ages clustering mainly at ~ 365 Ma and 450–520 Ma (Fig. S2). Subordinate Precambrian zircons show a major age population around 700–1000 Ma and several peaks between 1.3 Ga and 3.4 Ga (Fig. S2). The Paleozoic zircons from the Lower Carboniferous samples have $\epsilon_{\text{Hf}}(t)$ values varying from -15.9 to $+15.7$, with the Late Paleozoic zircons showing higher $\epsilon_{\text{Hf}}(t)$ values (-5.4 to $+13.5$). In contrast, the Precambrian ones are characterized by a larger spread of $\epsilon_{\text{Hf}}(t)$ values between -21.7 to $+18.2$ (Fig. S3; Table S2).

Discussion

Precambrian detritus in the Junggar and Altai terranes from the siberian continent

In the Junggar terrane, the middle Devonian–Carboniferous sedimentary rocks show similar U–Pb age spectrum of detrital zircons with the older, Silurian–early Devonian strata, suggesting prolonged sedimentary recycling (Fig. 4a). The detrital zircons for the Silurian–Carboniferous rocks span a nearly continuous Archean–Paleozoic age range from 311 to 3539 Ma, clustering around four main Precambrian populations at 700–1000 Ma, 1.2–1.4 Ga, 1.8–2.1 Ga and 2.3–2.9 Ga (Fig. 4a). These Precambrian zircons have little possibility to derive from the Junggar terrane because it lacks ancient basement rocks²⁴. In particular, abundant ~ 820 and ~ 930 Ma detrital zircons occur in the strata (Fig. 4a) but contemporaneous magmatic rocks are absent in this region. High pspicity of the Precambrian zircons (Fig. S1) indicates that the old detritus in the Silurian–Carboniferous strata more likely represent allochthonous components that shed onto the Junggar terrane via a long-distance transportation during Silurian–early Devonian time.

Precambrian magmatic rocks are widely exposed in the Tarim craton and adjacent CTB and YB, but the 500–600 Ma, 1.2–1.4 Ga and 2.6–2.9 Ga magmatic events that are prevailed in detrital zircons from the Junggar

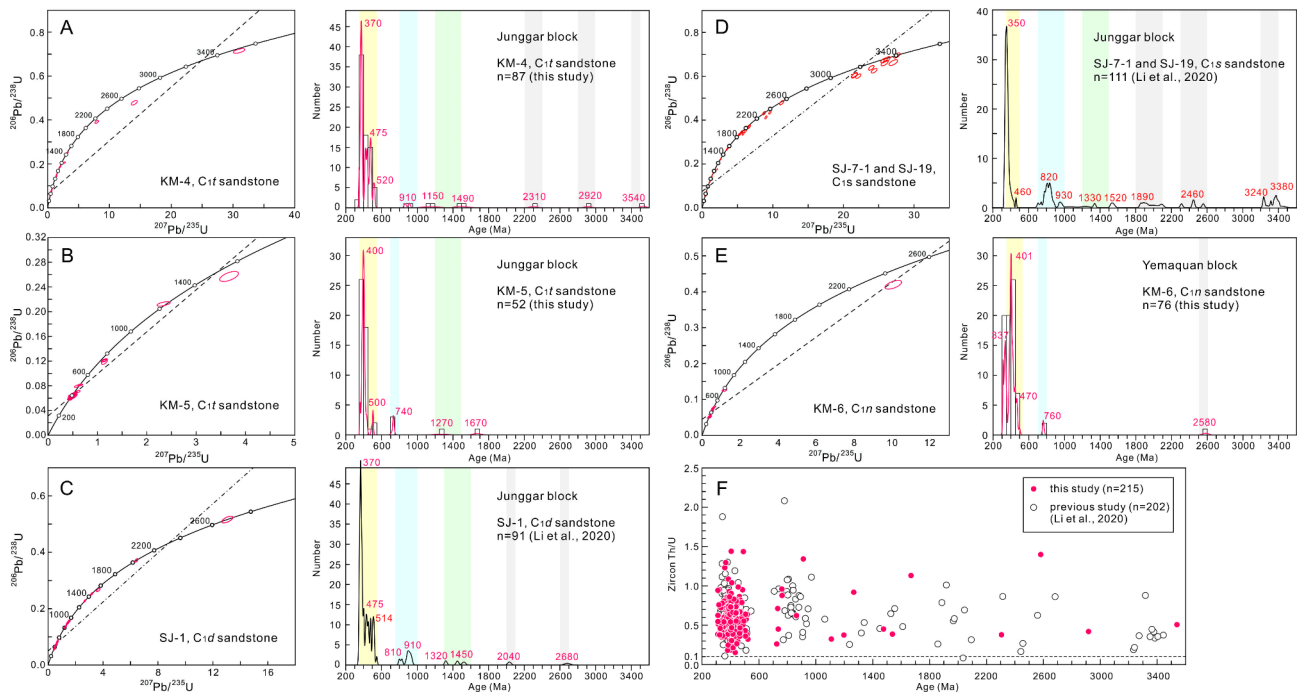


Fig. 3. Detrital zircon U–Pb concordant diagrams of the Lower Carboniferous sandstone samples from the northern margin of the Junggar block and the southern margin of the Yemaquan block. The compared detrital zircon U–Pb age distribution for the Lower Carboniferous Tamugang Formation sandstone (SJ-1) is from Li et al.³³.

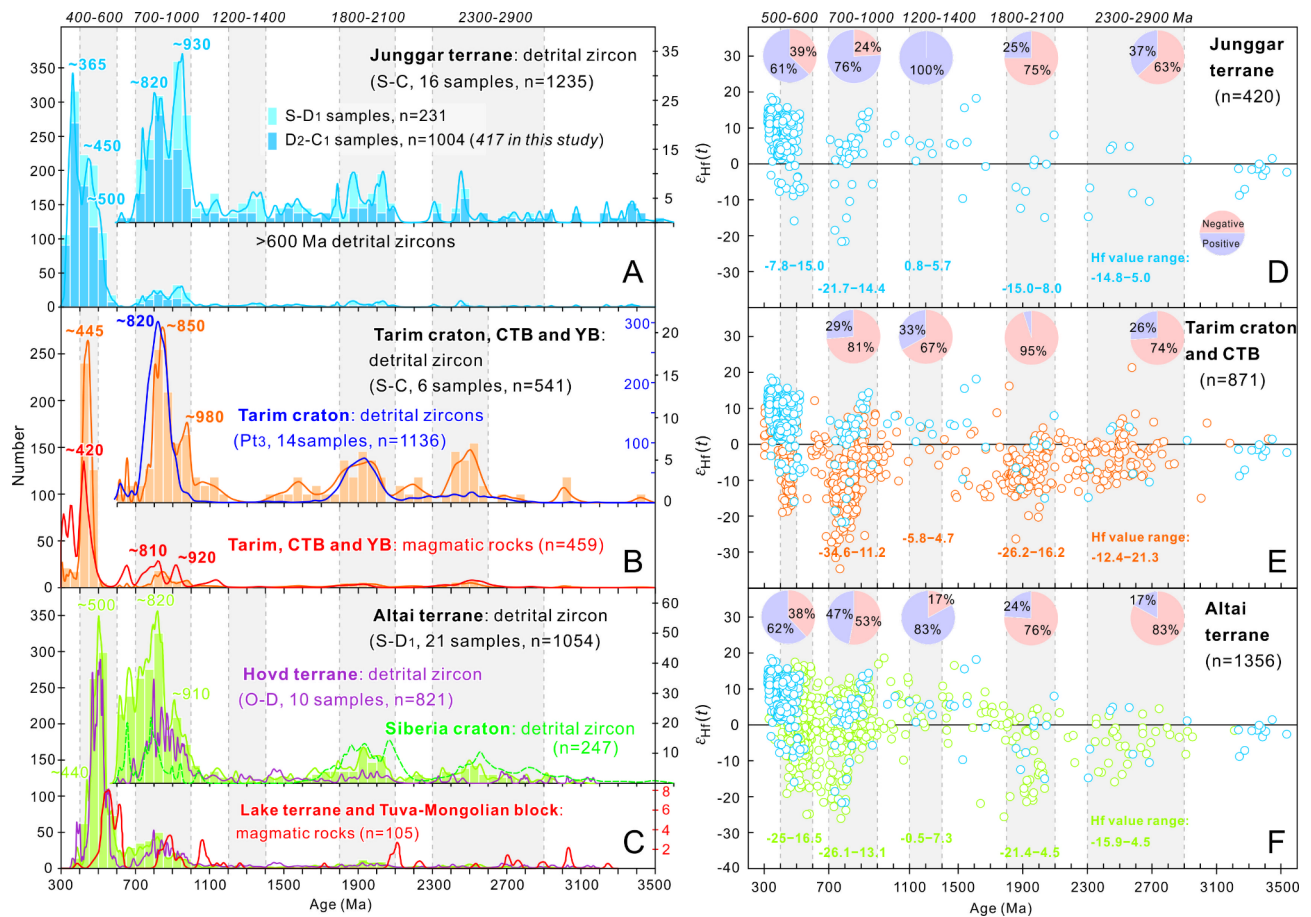


Fig. 4. (a–f) Age distributions and Hf isotopic compositions of the detrital zircons from the Silurian–Carboniferous strata in the Junggar terrane, the Tarim craton and neighbors, and the Altai terrane, respectively. The age distribution curves of the Precambrian (> 600 Ma) detrital zircons are shown for comparison, including those from the Neoproterozoic and the Silurian–Carboniferous strata in the Tarim craton, the Ordovician–Devonian strata in the Hovd terrane, and the Neoproterozoic strata in the Siberia craton. See Tables S6 for the U–Pb–Hf data sources of the detrital zircons. The compiled crystallization ages of the magmatic rocks in the Tarim craton and neighbors and in the Lake terrane and the Tuva–Mongolian microcontinent are from Han et al.²⁰ and Soejono et al.¹⁵, respectively.

terrane are essentially lacking or rather weak (Fig. 4b). The lack of these magmatic episodes is manifested by detrital zircon records in both Neoproterozoic and Silurian–Carboniferous strata (Fig. 4b). Furthermore, the 700–1000 Ma zircons in the Tarim and neighbors show $\epsilon_{\text{Hf}}(t)$ values ranging from -34.6 to 11.2 (81% negative values) (Fig. 4e), different from the range of -21.7 to 14.4 of those coeval zircons (24% negative values) in the Junggar terrane (Fig. 4d). In addition, numerous studies endorse the existence of a Paleozoic oceanic basin between the Junggar terrane and the CTB³⁴, preventing the sediment transportation. These features suggest that the Tarim craton may not be the provenance of the Precambrian detritus in the Junggar terrane.

Instead, the Silurian–early Devonian strata in the Altai terrane show a comparable detrital zircon age spectrum with those in the Junggar terrane (Fig. 4a, c). The spectrum displays the 400–600 Ma, 700–1000 Ma, 1.2–1.4 Ga, 1.8–2.1 Ga and 2.3–2.6 Ga populations and the ~440 Ma, ~500 Ma, ~820 Ma and ~910 Ma peaks (Fig. 4c). Furthermore, the zircon $\epsilon_{\text{Hf}}(t)$ values and positive/negative values proportions of the Precambrian age populations in the Altai terrane are broadly identical to the coeval ones in the Junggar terrane. Both the Altai terrane and the Junggar terrane are characterized by predominant positive $\epsilon_{\text{Hf}}(t)$ values for the 1.2–1.4 Ga zircons (Fig. 4d, f). More importantly, the distinctive 500–600 Ma zircons in the Altai and Junggar terrane show an overlapped range of $\epsilon_{\text{Hf}}(t)$ values (-25.0 to 16.5 and -7.8 to 15.0), and a consistent negative value proportion (62% and 61%) (Fig. 4d, f). The above similarities, together with same storage horizon (i.e., Silurian–early Devonian strata), indicate that the Precambrian detrital materials in the Junggar and Altai terranes share a common provenance. It has been documented that the Precambrian magmatic events on the Siberia craton occurred spanning from the Archean to the Neoproterozoic and cluster in three major periods: 540–1000 Ma, 1.7–2.2 Ga, and 2.4–2.9 Ga^{35,36} (Fig. 4c). These three periods of magmatism define a $\epsilon_{\text{Hf}}(t)$ value range from -22.6 to 13.3 for the 700–1000 Ma zircons, from -20 to 7 for the 1.8–2.1 Ga zircons, and from -15 to 5 for the 2.3–2.6 Ga zircons^{37,38}. Such age and Hf isotope brackets correspond well with those of the Precambrian detrital zircons from the Junggar and Altai terranes, indicating that the Siberia craton was an important source.

In addition, both the Junggar and Altai terranes exhibit a similar age distribution pattern with the Hovd terrane (Fig. 4a, c), especially for the Neoproterozoic zircons, suggesting that the Mongolian collage system might also contribute the old detritus³⁹. Firstly, the ca. 460–570 Ma and ca. 750–950 Ma magmatic activities have been reported in the Lake terrane and the Tuva-Mongolian, Zavkhan and Baydrag blocks⁵ (Fig. 4c), and these rocks have a capability of providing some Neoproterozoic clastic materials¹⁷. More importantly, minor 1.0–1.7 Ga zircons in two terranes, which are obviously absent in the Siberia craton (Fig. 4c), could be derived from the Precambrian basement of the Mongolian continental blocks^{40,41}. These correlations enable us to argue that the Precambrian detrital materials in the Junggar and Altai terranes most likely came from the Siberia craton, with contributions from the Tuva-Mongolian microcontinent.

Mid-paleozoic tectonic link between the Junggar and Altai terranes

Oceanic subduction at convergent margins controls magmatic generation and evolution in the upper plate, and the major change of the accretionary regime can be revealed by the variation of zircon Hf isotopic compositions^{42,43}. Compiled U–Pb–Hf isotopic data for the Paleozoic zircons from the sedimentary and magmatic rocks in the Junggar terrane show a marked change of $\epsilon_{\text{Hf}}(t)$ values at ca. 420–410 Ma, with a wide range (-17 to +16) between 520 and 420 Ma, contrasting with the predominantly positive $\epsilon_{\text{Hf}}(t)$ values (+2 to +18) for ca. 410–350 Ma zircons (Fig. 5b). We interpret such a zircon Hf isotopic change at ca. 420–410 Ma as an accretionary tectonic transition from an advancing to retreating mode. This is because the advancing accretion could induce crustal compression and thickening and thus greater contribution of crustal materials into magmas with a decreasing trend of zircon $\epsilon_{\text{Hf}}(t)$ values⁴². In contrast, the retreating accretionary process would enhance the input of mantle materials by the resultant crustal extension and cause a gradual increase of zircon $\epsilon_{\text{Hf}}(t)$ values^{43,44}. This tectonic switching event at ca. 420–410 Ma in the Junggar terrane is manifested by the generation of extension-related magmatic rocks including the Early Devonian Well LC1 basaltic rocks within the Junggar Basin²³ (Fig. 1b) and granitic intrusions in the Yemaquan block³¹, which was synchronous with those occurred in the Chinese Altai terrane⁴⁵.

Both the Junggar terrane and the northern Tarim craton were in the advancing accretionary stage since the Late Cambrian, but the former experienced an accretionary tectonic shift markedly earlier than the latter that happened at ca. 400 Ma⁴⁶ (Fig. 5b). Furthermore, the Junggar terrane is dominated by the Early Paleozoic volcano-sedimentary successions, with the development of numerous Ordovician–Silurian arc magmatic rocks constituting the Dananhu arc along the southern margin of the Junggar block³⁴. This contrasts with the Cambrian–Ordovician carbonate-clastic deposition on the northern Tarim craton and its neighbors. These discrepancies demonstrate the existence of a northward oceanic subduction beneath the Junggar terrane during early Paleozoic time, similar to the case of the Altai terrane²⁷. However, in view of the inconsistent oldest arc magmatic record (Fig. 5c), the two regions were likely related to different subducting branches of the PAO at that time (Fig. 6a). The advancing subduction in the Junggar region may result in the closure of the Karamaili Ocean and amalgamation of the Junggar and Yemaquan blocks during the late Ordovician–Silurian to form the unified Junggar terrane²². Given that the Junggar terrane received the Precambrian detritus from the Siberia continent coevally with the Altai terrane, and the depositional ages of the Silurian–early Devonian rocks in both terranes that preserves these old materials have been constrained to be ca. 440–410 Ma^{13,26}, we propose that the Junggar terrane had collided with the Altai terrane at that time. This consideration is corroborated by the concurrence of tectonic contraction and related crustal thickening in the two terranes^{22,47}, as well as a dramatic decrease of zircon $\epsilon_{\text{Hf}}(t)$ values in the Altai terrane that more likely corresponds to a collision event⁴⁸ (Fig. 5a). Geological responses to this collisional event are expressed by the deformation/metamorphism of the Early Paleozoic strata spanning from the Junggar to Altai terrane and a regional unconformity on top of the strata^{26,49,50}. Ca. 430–420 Ma metamorphic event has been determined in the Chinese Altai^{51,52}. All of the above evidence supports a mid-Paleozoic collisional event between the Junggar terrane and the Altai terrane during the advancing accretionary orogenesis (Fig. 6b). Following the tectonic transition at ca. 420–410 Ma, the Junggar–Altai region underwent an intense and rapid extension. This tectonic regime is expressed by the early Devonian crustal thinning in the Junggar terrane²² and extension-related sub-horizontal foliation structure in the Altai terrane⁵³. Voluminous Early Devonian rift magmatism occurred in the broad region of Junggar to western Mongolia, with the generation of ca. 398 Ma basaltic rock in the Junggar Basin²³, ca. 413 Ma leucogranite in the Yemaquan arc³¹, and ca. 415–390 Ma bimodal volcanic suites in the Altai and Sayan terranes^{54,55}. Moreover, the Lower Devonian transgressive depositional successions in the Junggar terrane also favor the extensional setting²⁹. Such an extensional event may lead to the opening of a series of oceanic basins in the Junggar–Altai region, as proved by 409–403 Ma ophiolitic record in the Zhaheba–Aermantai/Irtysh and Karamaili suture zones (Fig. 5c). A notable feature is that the Middle Paleozoic arc magmatism of the Junggar block migrated to its southern margin (i.e., Dananhu) in the late Silurian, indicates that the ca. 420–410 Ma accretionary tectonic switch was likely driven by the rollback of the subducting PAO plate (Fig. 6c). These results demonstrate that, following the dock of Tuva-Mongolian microcontinent to the Siberian margin¹⁸, the Junggar terrane had been accreted to the Altai-Mongolian terrane in the mid-Paleozoic, which is temporally consistent with the amalgamation among the Gorny Altai, Altai-Mongolian and West Sayan terranes^{17,18}.

Implications for tectono-paleogeographic reconstruction in central Asia

Our work links the mid-Paleozoic source-to-sink sedimentary system with accretionary tectonic events in the Junggar–Altai region. Their spatio-temporal relationships unravel a short-lived connection between the Junggar and Altai terranes, possibly during the late Ordovician–Silurian, which provides new insights into Paleozoic tectonic reconstruction in central Asia. The Junggar terrane is a small but important tectonic component of the CAOB², and its tectono-paleogeographic framework, especially during the Early Paleozoic, always lacks available constraints. Numerous studies have shown that the Junggar terrane is underlain predominately by juvenile crust,

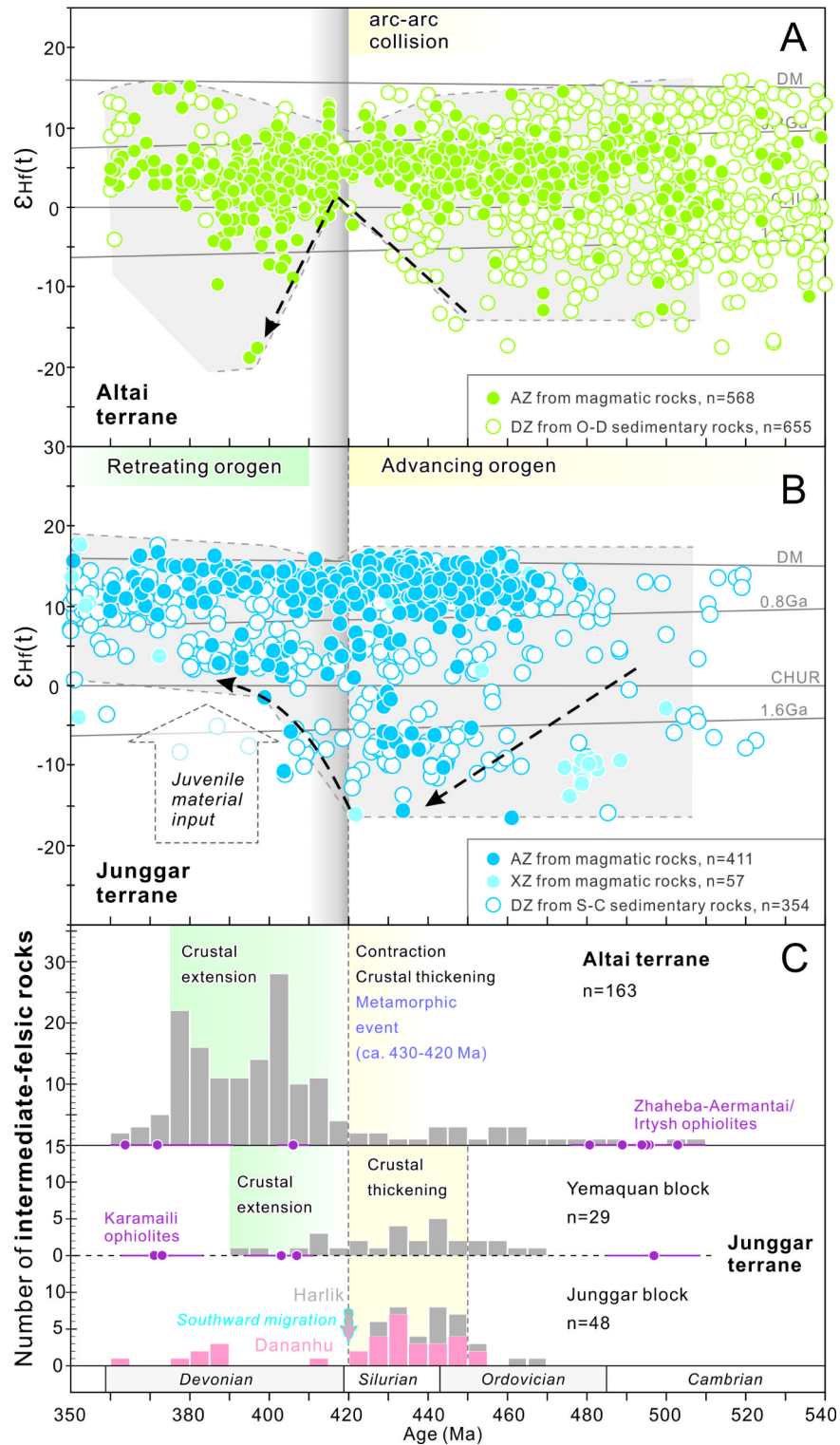


Fig. 5. (a-b) Plot of $\epsilon_{Hf}(t)$ values versus U-Pb ages of detrital and magmatic zircons from the Altai terrane (compiled data by Li et al.²²) and the Junggar terrane (this study; Tables S4,S5). (c) Summary of mid-Paleozoic key geological records in the Junggar and Altai terranes concerning tectonic regime^{22,47}, metamorphic event^{51,52} and magmatic distribution (see Table S3 for data sources), as well as the ages of the ophiolitic rocks along the Karamaili, Zhaheba-Aermantai and Irtysh suture zones²².

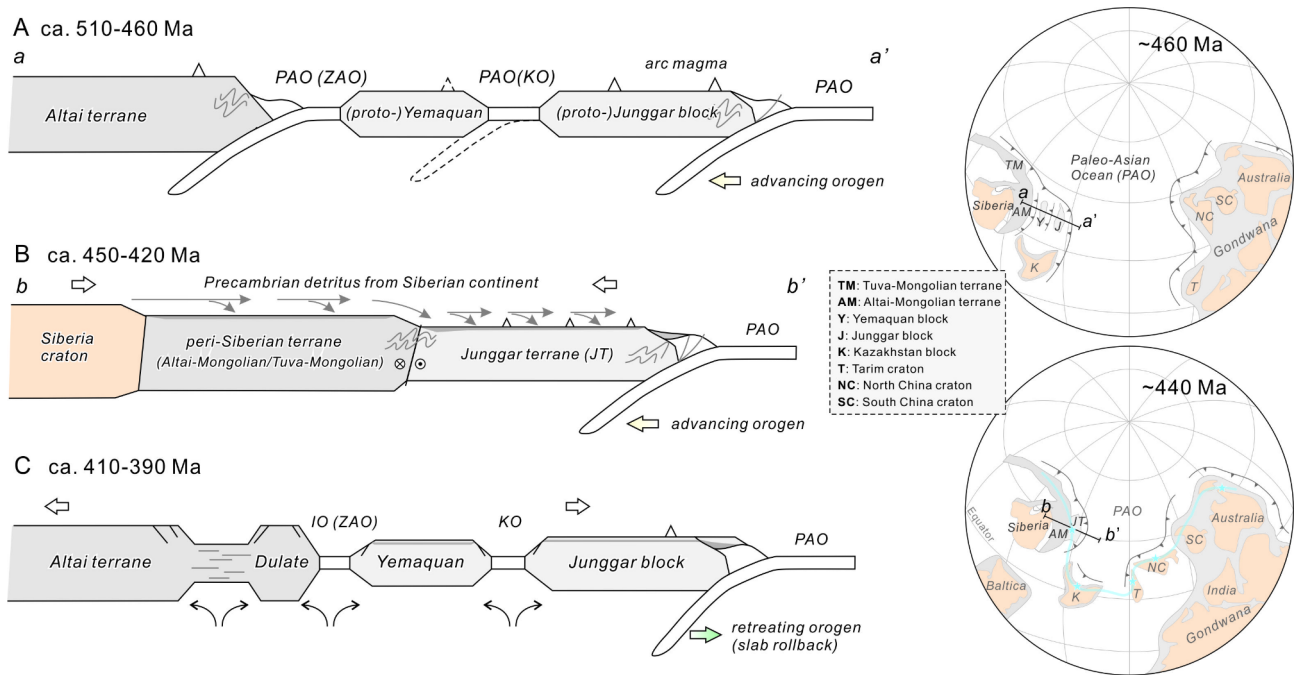


Fig. 6. Sketch illustrations (not to scale) showing accretionary tectonic evolution of the Junggar terrane, and its amalgamation and dispersion with the Altai terrane in the global plate reconstruction during mid-Paleozoic time. See text for details. ZAO—Zhaheba-Aermantai Ocean; KO—Karamaili Ocean. This figure is generated using CorelDRAW X8 created by the CorelDRAW Team under an open license (<http://www.coreldraw.com/cn/product/graphic-design-software/>).

possibly with a very limited ancient basement^{22,24}. Our results suggest that it did not receive the detrital materials from the Tarim craton that was located on the Gondwana northern margin in the Early Paleozoic⁴⁶. Furthermore, the characteristic 500–600 Ma detrital zircons in the Junggar terrane have predominant positive $\varepsilon_{\text{Hf}}(t)$ values contrasting with those more evolved Hf isotopic compositions from the Neoproterozoic–Early Paleozoic strata in the North Indian, Australian and North African terranes⁵⁶. These indicate that the Junggar terrane was not derived from the Gondwana and unconnected with the Tarim craton prior to their final amalgamation in the late Paleozoic. Instead, it was more likely to reside in the northern hemisphere all the time, and lie in the PAO realm adjacent to the peri-Siberian accretionary margin during the Early Paleozoic (Fig. 6). The determination of advancing subduction-induced terrane accretion event not only reveals the mid-Paleozoic tectonic affinity of the Junggar terrane and the peri-Siberian accretionary system (Fig. 6b), but also defines an Early Paleozoic paleogeographic boundary for the CAO roughly between the Junggar block and the CTB (i.e., North Tianshan suture zone; Fig. 1b) that can extend to the Solonker suture zone. Such a division scheme is supported by the distribution of Silurian *Tuvaella* brachiopod fauna⁵⁷, different from that for Late Paleozoic one along the South Tianshan–Solonker suture zone². Divergent double subduction of the PAO plate has been shown to govern the accretionary evolution of the Siberian margin to the north and the Gondwana continent to the south during the Early Paleozoic⁵. The middle Paleozoic switching accretionary tectonics that is recognized in the Junggar–Altai region commonly took place in the peri-Siberian terranes^{16,18}, the eastern Kazakhstan block⁵⁸ and the Gondwana marginal blocks such as northern Tarim and northern North China⁴⁶. These together constitute an accretionary orogenic girdle above the PAO subduction zone at that time, which is reconciled with the global plate reconstruction by Merdith et al.⁵⁹. The advancing accretion brings a kinematic constraint that the Siberia and Gondwana may proceed a northward drift during the Early Paleozoic, at least after the final assembly of Gondwana at ~500 Ma^{60,61}. The subsequent retreating accretion since the early Devonian is more likely to induce the breakup of Gondwana^{6,46} and the building of the Late Paleozoic archipelago geographic framework in the PAO realm². Additionally, we reveal the Caledonian-age tectonic evolution in the southwestern CAO connecting the Neoproterozoic and Late Paleozoic accretionary history at the periphery of Siberia and link it with those concurrently along the circum-PAO accretionary margin. The Paleozoic accretionary tectonics have been documented to spatially overlap the Neoproterozoic ones along the Kazakhstan eastern margin and the Gondwana northern margin^{18,19}. These support that the PAO was not a newborn ocean but represent a remnant of the Ran-Rodinia Ocean⁵. Therefore, its long-lived subduction during the Neoproterozoic to Paleozoic and final closure possibly governed the evolution from Rodinia to Gondwana⁶² and the development of the CAO¹.

Conclusion

This study uses detrital zircon U–Pb–Hf data to investigate the provenance of the Precambrian sedimentary materials in the Junggar terrane and related tectonic factor. Our results manifest that the Precambrian detritus in the Junggar terrane shares a single provenance with those in the Altai terrane and they are derived from

the Siberian continent. The Junggar terrane underwent a mid-Paleozoic accretionary tectonic switch from an advancing to retreating mode. The advancing subduction induced the amalgamation of the Junggar terrane with the Altai terrane during the Silurian–early Devonian, allowing the transportation of old detritus from the Siberia craton and adjacent Tuva-Mongolian microcontinent. These findings help to delineate an Early Paleozoic tectono-paleogeographic boundary of the CAOBS along the North Tianshan–Solonker suture zone. In combination with regional tectonic correlation, we suggest that the PAO is a long-lived ocean representing a remnant of the Ran-Rodinia Ocean, with its protracted subduction governing the Neoproterozoic–Paleozoic accretionary orogenic evolution throughout the Siberia southern margin (present coordinates), the Kazakhstan eastern margin and the Gondwana northern margin.

Sample and analytical methods

This study established the Paleozoic connection among the Junggar terrane, Altai terrane and Siberian craton by examining their source-to-sink sedimentary and accretionary tectonic correlation, based on new and compiled zircon U–Pb–Hf data from the three regions. They included 2289 radiometric ages and 1776 zircon $\varepsilon_{\text{Hf}}(t)$ isotopic analyses from the Junggar and Altai terranes, as well as 2498 zircon U–Pb dating results with 871 $\varepsilon_{\text{Hf}}(t)$ values from the Tarim and Siberian cratons and their neighbors. See the supplementary information for sample description and (our and compiled) analytical data used in this study.

Zircon U–Pb dating

Zircons were separated from samples processed by crushing, heavy-liquid, and magnetic methods and then were mounted in epoxy resin and polished to expose the interior. Cathodoluminescence images were used to examine the internal structures of zircons prior to isotopic analysis. In-situ zircon U–Pb dating was carried out at the Northwest University in Xi'an, China, using a laser ablation-inductively coupled plasma-mass spectrometry (LA–ICP–MS) assembled with a GeoLas 200 M ArF–excimer 193 nm laser ablation system and an Agilent 7500a quadrupole ICP–MS. Laser frequency was 10 Hz and spot sizes were between 30 and 40 μm . A carrier gas (high-purity helium) was mixed with a make-up gas (high-purity argon) before entering the ICP–MS to achieve stable and optimum conditions, resulting in negligible contribution of ^{204}Hg to ^{204}Pb (count rate of the mass 204 for blank < 100 counts per second). The Harvard zircon 91,500 was used as a standard for isotopic ratio corrections. The GLITTER 4.0 program (Macquarie University) was used to process raw count data to obtain U–Th–Pb isotopic ratios and elemental concentrations. U, Th and Pb contents were calculated by using NIST SRM 610 as an external standard and ^{29}Si as an internal standard. Common Pb was corrected using the ComPbCorr program (ver. 3.16e)⁶⁴. Zircon standard GJ-1 analyzed as an unknown yielded a weighted mean $^{206}\text{Pb}/^{238}\text{U}$ age of 601.0 ± 3.6 Ma (MSWD = 2.9, $n = 45$), which is consistent with the TIMS age of 600.4 ± 0.6 Ma⁶⁵. Detailed instrumental settings and analytical procedures also refer to Diwu et al.⁶⁶ and Liu et al.⁶⁷. The Excel macros “NORMALIZED PROB PLOT” 2/3 created by G. Gehrels at the University of Arizona was used for age data statistics and presentation (Arizona LaserChron Center: <https://sites.google.com/a/laserchron.org/laserchron/>).

Zircon Lu–Hf isotope analysis

Zircon Hf isotopes for the Carboniferous sandstones were analyzed at the Northwest University in Xi'an, China, and determined using a Nu Plasma II MC–ICP–MS and a RESOLUTION M-50 (ASI) excimer ArF laser ablation system all housed at the SKLCD, Northwest university in Xi'an, China. The laser ablation system (RESOLUTION M-50, ASI) consisted of an excimer laser (193 nm), a two-volume laser ablation cell (Laurin Technic S155, 155 mm \times 105 mm), a Squid smoothing device, and a computer-controlled high-precision X–Y stage. The two-volume laser ablation cell was designed to avoid cross contamination and reduce background flushing time, while the Squid smoothing device could give a smooth signal with laser pulse rates down to 1 Hz. Sensitivity and fractionation were independent of the sampling position in the cell. Helium was used as a carrier gas for the laser ablation process, and it entered the cell body at its bottom to fill the big cell. Helium from both bottom and argon from the funnel cell were admixed downstream, in front of the squid signal smoothing device, into the MC–ICP–MS. The Nu Plasma multi-collector ICP–MS system (Nu plasma II, Nu Instruments Wrexham, UK) used for Hf analysis represents the latest generation of double-focusing mass spectrometers. The new collector has sixteen Faraday detectors for greater flexibility, and its five full-size discrete dynode multipliers enable the determination of precise isotope ratios, even for isotopes with very low abundance. Its zoom optics system allows the observation of instant changes in dispersion and perfect peak overlap, without slow and potentially unreliable detector movement. In this study, the ion beams of ^{180}Hf , ^{179}Hf , ^{178}Hf , ^{177}Hf , $^{176}\text{Hf}+^{176}\text{Yb}+^{176}\text{Lu}$, ^{175}Lu , ^{174}Yb , ^{173}Yb , ^{172}Yb , ^{171}Yb were collected in Faraday cups H4, H3, H2, H1, Ax, L1, L2, L3, L4, L5, respectively. Among the measured isotopes, the $^{179}\text{Hf}/^{177}\text{Hf}$ ratio was applied to calculate the mass fractionation of Hf (β_{Hf}), the ^{175}Lu signal and $^{176}\text{Lu}/^{175}\text{Lu}=0.02656$ were used to calculate the interference of ^{176}Lu on ^{176}Hf . ^{173}Yb – ^{171}Yb was applied to calculate both β_{Yb} , and the ^{173}Yb signal and $^{176}\text{Yb}/^{173}\text{Yb}=0.78696$ were used to calculate the interference of ^{176}Yb on ^{176}Hf . The detail information of analysis strategy and data deduction can be found in published literature⁶⁸.

Calculation of Hf parameters

Zircon initial $^{176}\text{Hf}/^{177}\text{Hf}$ ratios were calculated using measured $^{176}\text{Lu}/^{177}\text{Hf}$ and $^{176}\text{Hf}/^{177}\text{Hf}$ ratios and a ^{176}Lu decay constant of $1.867 \times 10^{-11} \text{ yr}^{-1}$ according to the method of Söderlund et al.⁶⁹. To calculate $\varepsilon_{\text{Hf}}(t)$ values, we adopted a present-day $^{176}\text{Lu}/^{177}\text{Hf}$ value of 0.0336 and a $^{176}\text{Hf}/^{177}\text{Hf}$ value of 0.282785 for the chondritic uniform reservoir (CHUR)⁷⁰. Depleted mantle model ages (T_{DM1}) were calculated with reference to a depleted mantle reservoir having present-day $^{176}\text{Lu}/^{177}\text{Hf}$ value of 0.0384 and $^{176}\text{Hf}/^{177}\text{Hf}$ value of 0.28325⁷¹. Crustal model ages (T_{DM2}) were calculated by assuming that the parental magma from which each zircon crystallized was originated from an average continental crust ($^{176}\text{Lu}/^{177}\text{Hf}=0.015$)⁷¹ which was derived from the depleted mantle.

Data availability

All data generated or analysed during this study are included in this published article and its supplementary information files.

Received: 6 June 2024; Accepted: 18 September 2024

Published online: 28 September 2024

References

- Windley, B. F., Alexeiev, D., Xiao, W. J., Kröner, A. & Badarch, G. Tectonic models for accretion of the central Asian Orogenic Belt. *J. Geol. Soc.* **164**, 31–47 (2007).
- Xiao, W. J. et al. A tale of amalgamation of three Permo-Triassic collage systems in Central Asia: Oroclines, sutures, and terminal accretion. *Annu. Rev. Earth Planet. Sci.* **43**, 477–507 (2015).
- Murphy, B. J. & Nance, D. *Pangea Conundrum Geol.* **36**, 703–706 (2008).
- Stampfli, G. M., Hochard, C., Vérard, C., Wilhema, C. & von Raumer, J. *Formaton Pangea Tectonophys.* **593**, 1–19 (2013).
- Zhao, G. C. et al. Geological reconstructions of the east Asian blocks: From the breakup of Rodinia to the assembly of Pangea. *Earth Sci. Rev.* **186**, 262–286 (2018).
- Metcalfe, I. Gondwana dispersion and Asian accretion: Tectonic and palaeogeographic evolution of eastern Tethys. *J. Asian Earth Sci.* **66**, 1–33 (2013).
- Dobretsov, N. L. & Buslov, M. M. Late Cambrian-Ordovician tectonics and geodynamics of Central Asia. *Russ. Geol. Geophys.* **48**, 71–82 (2007).
- Wilhem, C., Windley, B. F. & Stampfli, G. M. The Altaids of Central Asia: A tectonic and evolutionary innovative review. *Earth Sci. Rev.* **113**, 303–341 (2012).
- Li, P. F. et al. Evolution of the central Asian Orogenic Belt along the siberian margin from neoproterozoic-early paleozoic accretion to devonian trench retreat and a comparison with phanerozoic eastern Australia. *Earth Sci. Rev.* **198**, 102951 (2019).
- Cocks, L. R. M. & Torsvik, T. H. The dynamic evolution of the palaeozoic geography of eastern Asia. *Earth Sci. Rev.* **117**, 40–79 (2013).
- Li, J. Y. Late neoproterozoic and paleozoic tectonic framework and evolution of eastern Xinjiang, NW China. *Geol. Rev. (Di Zhi Lun Ping)*. **50**, 304–322 (2004).
- Li, Y. P., Li, J. Y., Sun, G. H., Zhu, Z. X. & Yang, Z. Q. Basement of Junggar basin: Evidence from detrital zircons in sandstone of previous devonian kalamaili formation. *Acta Petrologica Sinica.* **23**, 1577–1590 (2007).
- Long, X. P. et al. Geochemistry and U–Pb detrital zircon dating of paleozoic graywackes in East Junggar, NW China: Insights into subduction-accretion processes in the southern central Asian orogenic belt. *Gondwana Res.* **21**, 637–653 (2012).
- Cawood, P. A., Hawkesworth, C. J. & Dhuime, B. Detrital zircon record and tectonic setting. *Geology.* **40**, 875–878 (2012).
- Soejono, I. et al. Early palaeozoic sedimentary record and provenance of flysch sequences in the Hovd Zone (western Mongolia): Implications for the geodynamic evolution of the Altai accretionary wedge system. *Gondwana Res.* **64**, 163–183 (2018).
- Chen, M. et al. Neoproterozoic–middle paleozoic tectono-magmatic evolution of the Gorny Altai terrane, northwest of the central Asian Orogenic Belt: Constraints from detrital zircon U–Pb and Hf-isotope studies. *Lithos.* **233**, 223–236 (2015).
- Cai, K. et al. Crustal nature and origin of the Russian Altai: Implications for the continental evolution and growth of the central Asian Orogenic Belt (CAOB). *Tectonophysics.* **674**, 182–194 (2016).
- Buslov, M. M., Shcherbanenko, T. A., Kulikova, A. V. & Sennikov, N. V. Palaeotectonic reconstructions of the central Asian folded belt in the silurian Tuvaella and Retziella brachiopod fauna locations. *Lethaia.* **55**, 1–15 (2022).
- Ge, R. F. et al. Neoproterozoic to paleozoic long-lived accretionary orogeny in the northern Tarim Craton. *Tectonics.* **33**, 302–329 (2014).
- Han, Y. et al. Paleozoic accretionary orogenesis in the Paleo-Asian Ocean: Insights from detrital zircons from silurian to Carboniferous strata at the northwestern margin of the Tarim Craton. *Tectonics.* **34**, 334–351 (2015).
- Badarch, G., Cunningham, W. D. & Windley, B. F. A new terrane subdivision for Mongolia: Implication for the phanerozoic crustal growth of Central Asia. *J. Asian Earth Sci.* **21**, 87–110 (2002).
- Li, D. et al. Arc-arc amalgamation during accretionary orogenesis: Insights from mid-paleozoic tectono-magmatic records in eastern Junggar, NW China. *Geosphere.* **20**, 407–420 (2024).
- Li, D., He, D. F. & Tang, Y. Reconstructing multiple arc-basin systems in the Altai–Junggar area (NW China): Implications for the architecture and evolution of the western central Asian Orogenic Belt. *J. Asian Earth Sci.* **121**, 84–107 (2016).
- Wang, T. et al. Quantitative characterization of orogens through isotopic mapping. *Commun. Earth Environ.* **4**, 110 (2023).
- Windley, B. F. et al. Neoproterozoic to paleozoic geology of the Altai Orogen, NW China: New Zircon age data and tectonic evolution. *J. Geol.* **110**, 719–739 (2002).
- Long, X. P. et al. Detrital zircon ages and hf isotopes of the early paleozoic flysch sequence in the Chinese Altai, NW China: New constrains on depositional age, provenance and tectonic evolution. *Tectonophysics.* **480**, 213–231 (2010).
- Jiang, Y. D. et al. Precambrian detrital zircons in the early paleozoic Chinese Altai: Their provenance and implications for the crustal growth of central Asia. *Precambrian Res.* **189**, 140–154 (2011).
- Yang, T. N., Li, J. Y., Zhang, J. & Hou, K. J. The Altai-Mongolia terrane in the central Asian Orogenic Belt (CAOB): A peri-gondwana one? Evidence from zircon U–Pb, hf isotopes and REE abundance. *Precambrian Res.* **187**, 79–98 (2011).
- Xu, Q. Q. et al. Early paleozoic arc magmatism in the Kalamaili orogenic belt, Northern Xinjiang, NW China: Implications for the tectonic evolution of the East Junggar terrane. *J. Asian Earth Sci.* **194**, 104072 (2020).
- Wang, T. et al. Timing, petrogenesis, and setting of paleozoic synorogenic intrusions from the Altai Mountains, Northwest China: implications for the tectonic evolution of an accretionary orogen. *J. Geol.* **114**, 735–751 (2006).
- Li, Y. P., Li, J. Y., Sun, G. H., Zhu, Z. X. & Song, B. Determination of the early devonian granite in East Junggar, Xinjiang, China and its geological implications. *Geol. Bull. China.* **28**, 1885–1893 (2009).
- Wan, B. et al. Contrasting styles of mineralization in the Chinese Altai and East Junggar, NW China: Implications for the accretionary history of the southern Altaids. *J. Geol. Soc.* **168**, 1311–1321 (2011).
- Li, D., He, D. F., Sun, M. & Zhang, L. The role of arc-arc collision in accretionary orogenesis: Insights from ~ 320 Ma tectono-sedimentary transition in the Karamaili area, NW China. *Tectonics.* **39**, 1–21 (2020).
- Chen, Z. et al. Composition, provenance and tectonic setting of the Southern Kangurtag accretionary complex in the Eastern Tianshan, NW China: Implications for the late paleozoic evolution of the North Tianshan Ocean. *Tectonics.* **38**, 2779–2802 (2019).
- Powerman, V., Shatsillo, A., Chumakov, N., Kapitonov, I. & Hourigan, J. Interaction between the central Asian Orogenic Belt (CAOB) and the siberian craton as recorded by detrital zircon suites from Transbaikalia. *Precambrian Res.* **267**, 39–71 (2015).
- Priyatkina, N. et al. The proterozoic evolution of northern siberian craton margin: A comparison of U–Pb–Hf signatures from sedimentary units of the Taimyr orogenic belt and the siberian platform. *Int. Geol. Rev.* **59**, 1632–1656 (2017).
- Priyatkina, N., Collins, W. J., Khudoley, A. K., Letnikova, E. F. & Huang, H. Q. The neoproterozoic evolution of the western siberian craton margin: U–Pb–Hf isotopic records of detrital zircons from the Yenisey Ridge and the Prisaayan Uplift. *Precambrian Res.* **305**, 197–217 (2018).

38. Priyatkina, N., Ernst, R. E. & Khudoley, A. K. A preliminary reassessment of the siberian cratonic basement with new U–Pb–Hf detrital zircon data. *Precambrian Res.* **340**, 105645 (2020).
39. Long, X. P. et al. Detrital zircon U–Pb ages and whole-rock geochemistry of early paleozoic metasedimentary rocks in the Mongolian Altai: Insights into the tectonic affinity of the whole Altai-Mongolian terrane. *Geol. Soc. Am. Bull.* **132**, 477–494 (2020).
40. Demoux, A. et al. D. Zircon ages from the Baydrag Block and the Bayankhongor Ophiolite Zone: Time constraints on late neoproterozoic to Cambrian subduction- and accretion-related magmatism in Central Mongolia. *J. Geol.* **117**, 377–397 (2009).
41. Bold, U., Crowley, J. L., Smith, E. F., Sambuu, O. & Macdonald, F. A. Neoproterozoic to early paleozoic tectonic evolution of the Zavkhan Terrane of Mongolia: implications for continental growth in the central Asian Orogenic Belt. *Lithosphere.* **8**, 729–750 (2016).
42. Kemp, A. I. S., Hawkesworth, C. J., Collins, W. J., Gray, C. M. & Blevin, P. L. Isotopic evidence for rapid continental growth in an extensional accretionary orogen: The tasmanides, eastern Australis. *Earth Planet. Sci. Lett.* **284**, 455–466 (2009).
43. Collins, W. J., Belousova, E. A., Kemp, A. I. S. & Murphy, J. B. Two contrasting phanerozoic orogenic systems revealed by hafnium isotope data. *Nat. Geosci.* **4**, 333–337 (2011).
44. Nelson, D. A. & Cottle, J. M. The secular development of accretionary orogens: Linking the Gondwana magmatic arc record of West Antarctica, Australia and South America. *Gondwana Res.* **63**, 15–33 (2018).
45. Sun, M. et al. Early paleozoic ridge subduction in the Chinese Altai: Insight from the marked change in Zircon Hf isotopic composition. *Sci. China Earth Sci.* **52**, 1345–1358 (2009).
46. Han, Y. G. et al. Tarim and North China cratons linked to northern Gondwana through switching accretionary tectonics and collisional orogenesis. *Geology.* **44**, 95–98 (2016).
47. Cui, X. et al. Geochronological and geochemical study of the high-grade orthogneissic rocks from the Northern Fuyun Complex: Implications for crustal architecture and Early-Middle Paleozoic evolution of the Chinese Altai. *Lithos* 366–367, 105547 (2020).
48. Smits, R. G., Collins, W. J., Hand, M., Dutch, R. & Payne, J. A. Proterozoic Wilson cycle identified by hf isotopes in central Australia: Implications for the assembly of Proterozoic Australia and Rodinia. *Geology.* **42**, 231–234 (2014).
49. He, G. Q. & Li, M. S. Significance of paleostructure and paleogeography of ordovician-silurian rock associations in Northern Xinjiang, China. *Acta Scientiarum Naturalium Universitatis Pekinensis (Beijing Da Xue Xue Bao Zi Ran Ke Xue Ban).* **37**, 99–110 (2001).
50. Wei, C., Clarke, G., Tian, W. & Qiu, L. Transition of metamorphic series from the Kyanite- to andalusite-types in the Altai orogen, Xinjiang, China: Evidence from petrography and calculated KFMASH and KFMASH phase relations. *Lithos.* **96**, 353–374 (2007).
51. Hu, A. Q., Wei, G. J., Deng, W. F. & Chen, L. L. SHRIMP zircon U–Pb dating and its significance for gneisses from the southeast area to Qinghe Country in the Altai, China. *Acta Petrologica Sinica.* **22**, 1–10 (2006).
52. Zhang, C. L. et al. Revisiting the Irtysh tectonic belt: Implications for the paleozoic tectonic evolution of the Altai orogen. *J. Asian Earth Sci.* **52**, 117–133 (2012).
53. Jiang, Y. D. et al. Barrovian and Buchan metamorphic series in the Chinese Altai: P-T-t evolution and tectonic implications. *J. Metamorph. Geol.* **40**, 823–857 (2022).
54. Chai, F. M. et al. Geochronology of metarhyolites from the Kangbutiebao formation in the Kelang basin, Altay Mountains, Xinjiang: Implications for the tectonic evolution and metallogeny. *Gondwana Res.* **16**, 189–200 (2009).
55. Vorontsov, A. et al. Magmatism of the devonian Altai-Sayan Rift System: Geological and geochemical evidence for diverse plume-lithosphere interactions. *Gondwana Res.* **89**, 193–219 (2021).
56. Wang, P. et al. Position of the Tarim Craton in Gondwana: Constraints from neoproterozoic to early paleozoic strata in South Tarim, NW China. *Tectonophysics.* **803**, 228741 (2021).
57. Rong, J. Y., Boucot, A. J., Su, Y. Z. & Strusz, D. L. Biogeographical analysis of late silurian brachiopod fauna, chiefly from Asia and Australia. *Lethaia.* **28**, 39–60 (1995).
58. Filippova, I. B., Bush, V. A. & Didenko, A. N. Middle paleozoic subduction belts: The leading factor in the formation of the central Asian fold- and- thrust belt. *Russ. J. Earth Sci.* **3**, 405–426 (2001).
59. Meredith, A. S. et al. Extending full-plate tectonic models into deep time: Linking the neoproterozoic and the Phanerozoic. *Earth Sci. Rev.* **214**, 103477 (2021).
60. Zhao, X. X. & Coe, R. S. Plate tectonics, China, in Gubbins, D., and Herrero-Bervera, E., eds., Encyclopedia of geomagnetism and paleomagnetism. *Amsterdam, Springer*, 816–828 (2007).
61. Huang, B. C. et al. Paleomagnetic constraints on the paleogeography of the east Asian blocks during late paleozoic and early mesozoic times. *Earth- Sci. Reviews.* **186**, 8–36 (2018).
62. Hoffman, P. F. Did the breakout of Laurentia turn Gondwanaland inside-out? *Science.* **252**, 1409–1412 (1991).
63. Chen, B. & Jahn, B. M. Genesis of post-collisional granitoids and basement nature of the Junggar Terrane, NW China: Nd–Sr isotope and trace element evidence. *J. Asian Earth Sci.* **23**, 691–703 (2004).
64. Andersen, T. Correction of common lead in U–Pb analyses that do not report ²⁰⁴Pb. *Chem. Geol.* **192**, 59–79 (2002).
65. Jackson, S. E., Pearson, N. J., Griffin, W. L. & Belousova, E. A. The application of laser ablation-inductively coupled plasma-mass spectrometry to in situ U–Pb zircon geochronology. *Chem. Geol.* **211**, 47–69 (2004).
66. Diwu, C. R. et al. Episodic tectonothermal events of the western North China Craton and North Qinling Orogenic Belt in central China: Constraints from detrital zircon U–Pb ages. *J. Asian Earth Sci.* **47**, 107–112 (2012).
67. Liu, X. M., Gao, S., Diwu, C. R. & Ling, W. L. Precambrian crustal growth of Yangtze Craton as revealed by detrital zircon studies. *Am. J. Sci.* **308**, 421–446 (2008).
68. Yuan, H. L. et al. Simultaneous determinations of U–Pb age, hf isotopes and trace element compositions of zircon by excimer laser-ablation quadrupole and multiple-collector ICP–MS. *Chem. Geol.* **247**, 100–118 (2008).
69. Söderlund, U., Patchett, P. J., Vervoort, J. D. & Isachsen, C. E. The ¹⁷⁶Lu decay constant determined by Lu–Hf and U–Pb isotope systematics of precambrian mafic intrusions. *Earth Planet. Sci. Lett.* **219**, 311–324 (2004).
70. Bouvier, A., Vervoort, J. D. & Patchett, P. J. The Lu–Hf and Sm–Nd isotopic composition of CHUR: Constraints from unequilibrated chondrites and implications for the bulk composition of terrestrial planets. *Earth Planet. Sci. Lett.* **273**, 48–57 (2008).
71. Griffin, W. L. et al. The hf isotope composition of cratonic mantle: LAM–MC–ICPMS analysis of zircon megacrysts in kimberlites. *Geochim. Cosmochim. Acta.* **64**, 133–147 (2000).

Acknowledgements

We are grateful to the Editor Dejan Prelevic and two anonymous reviewers for their constructive comments and suggestions. This research was supported by the National Natural Science Foundation of China (No. 42172124, No. 41702110, No. 41730213, No. 42330810, and No. U19B6003-01) and the National Key R&D Program of China (No. 2023YFF0804302). This work is a contribution to IGCP 662.

Author contributions

D.L. and Y.G.H. were involved in designing the study, analyzing the data, and writing the manuscript. G.C.Z., M.F.Z. and D.F.H. evaluated the results and conclusions and assisted with manuscript preparation and revision.

S.Q.H., Y.Z., D.F. and H.Y. contributed to collection and geochronological and Lu–Hf isotopic analyses of the rock samples, and manuscript editing. All authors reviewed the manuscript.

Declarations

Competing interests

The authors declare no competing interests.

Additional information

Supplementary Information The online version contains supplementary material available at <https://doi.org/10.1038/s41598-024-73532-3>.

Correspondence and requests for materials should be addressed to D.L. or Y.H.

Reprints and permissions information is available at www.nature.com/reprints.

Publisher's note Springer Nature remains neutral with regard to jurisdictional claims in published maps and institutional affiliations.

Open Access This article is licensed under a Creative Commons Attribution-NonCommercial-NoDerivatives 4.0 International License, which permits any non-commercial use, sharing, distribution and reproduction in any medium or format, as long as you give appropriate credit to the original author(s) and the source, provide a link to the Creative Commons licence, and indicate if you modified the licensed material. You do not have permission under this licence to share adapted material derived from this article or parts of it. The images or other third party material in this article are included in the article's Creative Commons licence, unless indicated otherwise in a credit line to the material. If material is not included in the article's Creative Commons licence and your intended use is not permitted by statutory regulation or exceeds the permitted use, you will need to obtain permission directly from the copyright holder. To view a copy of this licence, visit <http://creativecommons.org/licenses/by-nc-nd/4.0/>.

© The Author(s) 2024